Research Article

Design of Wideband Two-Sided Bandpass Frequency Selective Surface for X, Ka, and Ku Band Application

V. Vanitha [ID],[1] S. Esther Florence [ID],[2] A. Alaguraj [ID],[3] and Lakshmi Janaki Gollamudi [ID][4]

[1]*Department of Electronics and Communication Engineering, Aarupadai Veedu Institute of Technology,*
 VMRF (Deemed to be University), Chennai, Tamil Nadu, India
[2]*Department of Electronics and Communication Engineering, College of Engineering, Guindy, Anna University, Chennai,*
 Tamil Nadu, India
[3]*Tata Consultancy Services, Chennai, Tamil Nadu, India*
[4]*Indian Institute of Science, Bangalore, India*

Correspondence should be addressed to V. Vanitha; vanitha.vlsi@gmail.com

A novel wideband bandpass frequency-selective surface functioning at X, Ku, and Ka bands is proposed in this article. The designed FSS has a metallic square loop and a circular ring, and they are printed on both sides of the FR4 substrate. The proposed design FR4-based single-layer FSS is operating from 11.075 GHz to 22.075 GHz with a fractional bandwidth of 66.36%. The parameters of the square loop and circular ring regulate the characteristics of the passband. The optimum dimension of these parameters is obtained with parametric analysis. The proposed structure is measured and fabricated. However, the measured results strongly agree with the simulated results, which authenticate the proposed design performance.

1. Introduction

In most RF circuits, the performance of the circuit totally depends on the characteristics of the filter. Such a filtering operation is performed by the frequency selective surface (FSS) [1] in a microwave wireless communication environment. FSS entails 2D or 3D structures with a definite period. The structure may be a slot or patch designed on a substrate made up of dielectric. Researchers widely use wideband FSS in many applications [2–5], including the radomes, Cassegrain antenna, shielding, absorbers, stealth applications, and so on, since most of the applications now operate over a wide operating range. Patch-based FSS achieves band stop performance, while bandpass performance is realized using slot-based FSS [1]. The major pullback limitation for the bandpass FSS is the narrow bandwidth [6–8]. The design and development of wideband bandpass FSS in the radomes and in the system with frequency reuse configuration, however, have had a significant research gap in recent years, according to the researchers. Few bandpass FSS with wideband are reported in [9]. There is great demand for wideband bandpass FSS in various applications. In the literature, few bandstop FSS [10, 11] and bandpass FSS [12, 13] are reported for the application, as mentioned earlier.

To improve the bandpass FSS bandwidth, the researchers intended to develop techniques like 2, 2.5, and 3D. The latter two [14–16] strongly attract investigators to the FSS design due to an additional degree of freedom compared to the 2D [17–20] topology. But the major limitations are the design and fabrication complexity. In [17], planar multilayer FSS is designed, but the high-quality factor results in narrow fractional bandwidth, and in [18], multilayer FSS with a stable Q factor consisting of the metal patch with wireframe is reported; it also results in a narrow band. A multilayer FSS can attain a maximum fractional bandwidth (FBW) of 20% by using nonresonant elements and adding more conducting layers to increase the bandwidth. Most of the 2D-based FSS results in narrow bandwidth due to the resonating behaviour. This can be overcome with nonresonant cascaded structures [21], and mushroom-shaped FSS with 15% FBW is reported in [22]. The hybrid unit cell is used to achieve FBW of 11.35%, as reported

in [22]. These two different structures are printed on adjacent sides of the substrates and have a high degree of design complexity. In [23], FSS based on a patch with VIA is designed, which offers FBW of 110%, and this structure has very poor band rejection characteristics, multilayer FSS with narrowband responses is reported in [24]. Another method of improving the bandwidth of the FSS is numerous steering conducting layers [25]. Even though the 63% FBW is achieved, the fabrication complexity is higher. The convoluting structures [26] are another approach, which can improve the bandwidth but has an asymmetric response due to different metallic topologies. In [27], metamaterial structure-based FSS is reported, but the gain is not stable in the operating X band. Triple band ultra-wideband FSS designed with symmetrical structures on either side of the substrate, wherein they are not identical structures [28]. It is possible to enhance the properties of frequency selectivity and miniaturisation by creating patches or etching slots. By incorporating slots and slits in the designed structure, it may increase the possibilities of wider range of applications.

Thereby, the proposed design performs as wideband (bandpass FSS). All the above methods in the literature can improve the bandwidth, but they also suffer from larger profiles, fabrication difficulties, and larger insertion loss.

In this article, a single-layer FSS with a wideband response is proposed for the X, Ku, and Ka band. The proposed FSS resonates at 16.5 GHz, and it has good stability under various incident angles. The unit cell has an overall dimension of $0.46 \lambda_0 \times 0.46 \lambda_0$. The structural parameters directly impact the resonance behaviour, and hence the optimum dimensions are obtained using the parametric analysis. The significance of the proposed FSS structure is mentioned below:

(1) The motivation of the proposed work is to reduce the reflections in the aircraft at a low cost, to design an FSS with minimum thickness for stealth applications, and to achieve wideband frequency. The proposed single-layer double sided FSS is compact with a minimum thickness and covers X, Ku, and Ka band with a fractional bandwidth of 66.36% as a wideband bandpass filter.

(2) The proposed prototype structure is fabricated and measured.

(3) The structure exhibits good angular and polarization stability in both TE and TM modes.

(4) On either side of the passband, the reflection coefficient is better than 20 dB.

Further, the structure of this manuscript is as follows: Section 2 describes the proposed unit cell design. Section 3 discusses parametric analysis with fuzzy verification. The fabricated proposed structure is compared with the measured and simulated results in Section 4. Finally, concludes the work by providing a summary in Section 5.

2. FSS Unit Cell Design and Analysis

On the FR4 substrate, a symmetrical square loop and circular patch are designed to produce a wide bandpass filter. Figure 1 depicts the proposed FSS unit cell geometry. On either side of

the substrate, the unit cell consists of a symmetrical square loop with a circular conducting ring. The white area in the front view of Figure 1 is the FR4 substrate region, and the metallic region is represented in the black colour area. On both sides of the FR4 dielectric substrate, the identical structure is printed. The $L1 = 11.9$ mm is the length of the metallic square loop's inner side; $L2 = 12.5$ mm is the length of the loop's outer side; and $R1 = 0.6$ mm is the radius of the circular conductive ring, which is employed as the identical structure of the unit cell. FR4 substrate of thickness $T1$ (0.4 mm) with loss tangent and 0.02 dielectric constant 4.4 and copper patch thickness $T2$ (0.035 mm) have been used. The optimum dimension of the critical parametric is finalized using parametric analysis. In Figure 1(a) the proposed FSS is shown in front and back views. In Figure 1(b), side view is shown, followed by the FSS design in the CST EM studio environment in Figures 1(c) and 1(d).

Fundamentally, frequency-selective surfaces are periodic structures distributed evenly in one or two dimensions to perform as filters, mostly the single unit cell dimension would be half of a wavelength [1]. By considering this, for the required frequency, the overall dimension is obtained. Meanwhile, by introducing additional square patches and rings the desirable frequency band is achieved. The evolution of each element and the improved results are plotted in Figure 1(e).

The proposed unit cell has a simple design using a simple circular ring and a symmetrical square loop. The symmetrical structure is chosen to obtain polarization stability at the unit cell level. The resonant frequency varied by changing its elements perimeter [29]. The Q factor is the reciprocal of the fractional bandwidth. $Q = f_{centre}/(f_2 - f_1)$. The Q factor for the proposed design is $Q = 1.4977$.

The full-wave simulation of the proposed FSS is performed using the CST software, and the unit cell boundary condition is used to replicate the infinite structure. Floquet ports are used for exciting the FSS. The transmission and reflection coefficients at various angles of incidence (AoI) for both polarization of TE and TM modes are presented in Figure 2. It has been noticed that the proposed FSS shows a stable resonance up to 45°. Beyond 45°, the shift in frequency is very low. The stable resonance stability at various AoI attributes to the unit cell's reduced overall size of $0.46 \lambda_0 \times 0.46 \lambda_0$. ($\lambda_0$—wavelength of free space @ lowest frequency). The angular stability of TM mode nearly achieves a stable response comparing to the minimum variation in TE mode. Since the incident wave of the E-field polarizes in Y-direction and H-field polarizes in X-direction this could cause a minor deviation in the output observed. Typically, the free space impedance of incidence for TE mode is the ratio of impedance and cosθ. Similarly, the E-field wave polarizes in X-direction, and the impedance of incidence in TM mode is the product of impedance and cosθ; hence, the H-field of the AoI is comparatively similar. It manifests a better response in TM mode compared to the TE mode polarizations [30]. With excellent stability in the resonant behaviour, the proposed FSS parameters such as $L1$, $L2$, $T1$, and $R1$ have excellent control over the passband. Further, in Section 3, the parameters of the simulated reflection coefficient of the proposed FSS are discussed.
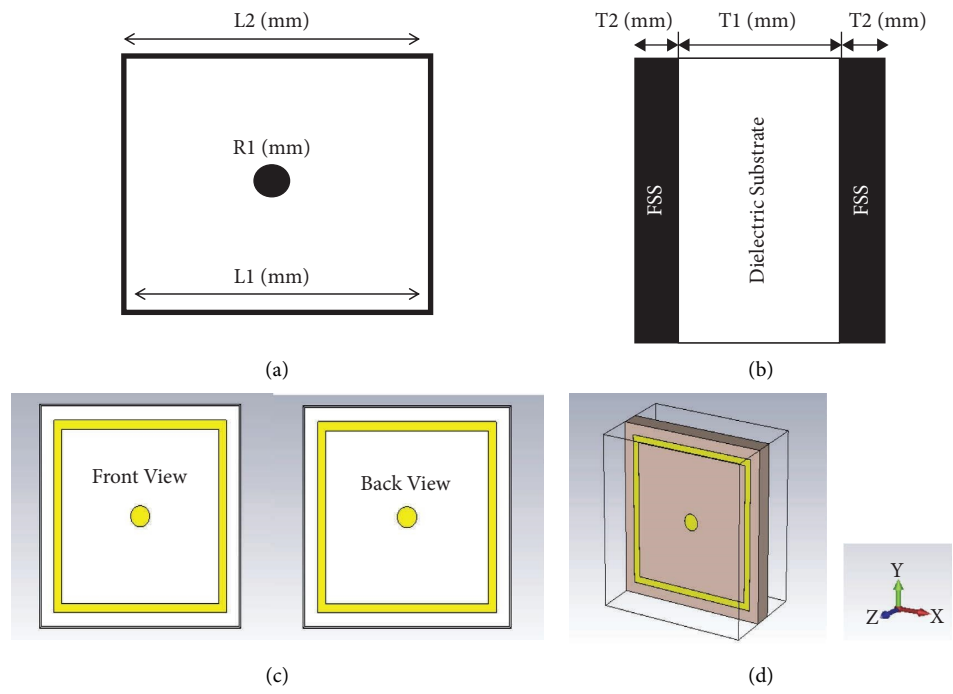
(a)

(b)

(c)

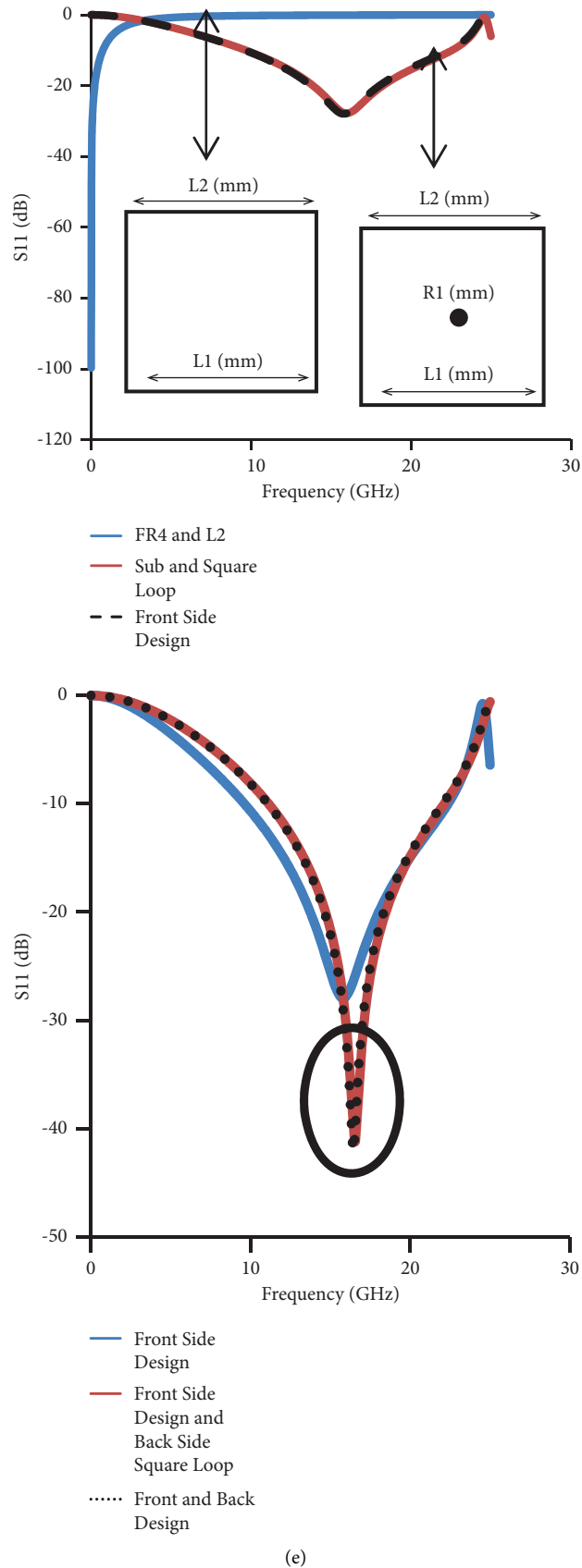(d)

Figure 1: Continued.

(e)

FIGURE 1: Structure of the proposed FSS. (a) Proposed FSS unit cell—front view and back view. (b) Proposed FSS unit cell—side view. (c) Front view and back view in CST environment. (d) Perspective view of the FSS. (e) Evolution of proposed unit cell.
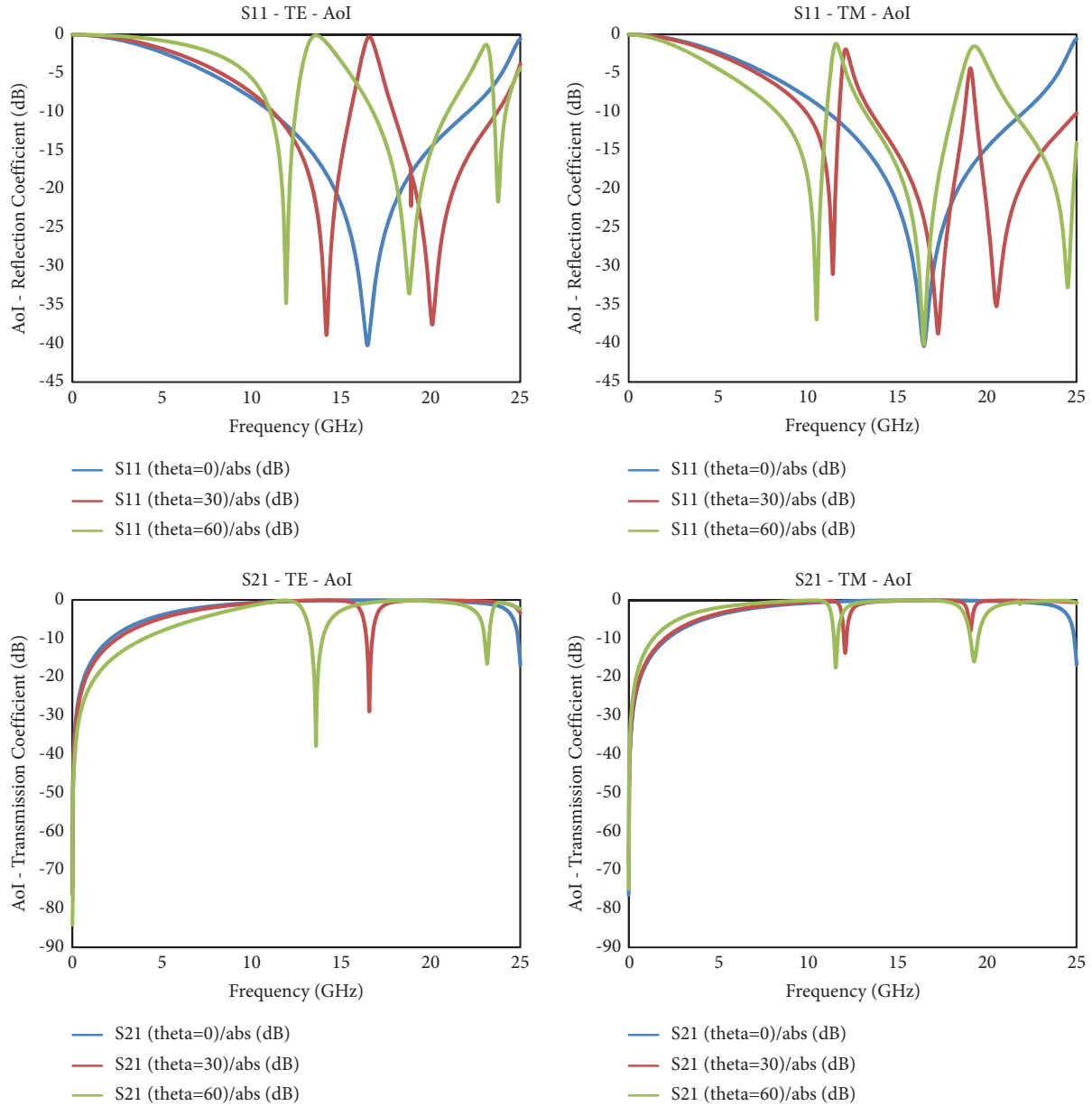
FIGURE 2: Transmission coefficient and reflection coefficient of TE and TM mode polarization for several AoI up to 60°.

3. Parametric Effect, Fuzzy Logic FBW Validation, and Equivalent Circuit of the Proposed FSS

Figure 3 shows the reflection coefficient of the proposed FSS for various $L1$ values. It is observed that the resonance frequency decreases with increasing patch length. Patch length reduction will result in a larger dielectric gap between the patches, decreasing the capacitance that increases the resonant frequency and providing a good correlation between the circumference of the ring and the effective wavelength at the resonance frequency. Hence, $L1 = 11.9$ mm is chosen for the final fabrication. In Figure 4, the reflection coefficient for various values of $L2$ is plotted, it is observed from the figure. As we increase the unit cell size, the transmission pole at 15.9 GHz is reduced, and

achieving good impedance bandwidth from 11.075 GHz to 22.075 GHz. Hence, $L2 = 12.5$ mm is chosen for the final fabrication. Figure 5 depicts the $S11$ of the proposed FSS for various $R1$ values. The figure shows that $R1 = 0.6$ mm has good impedance bandwidth since the large ring will provide a larger current path, increasing the wavelength and reducing the frequency. From Figure 6, it is observed that $T1 = 0.4$ mm features effective impedance matching, and hence it is chosen for the final fabrication. By varying the values of the parameters, we have achieved a better fractional bandwidth of 66.36% for both the TE and TM modes of reflection coefficient ($S11$).

The optimum dimensions for the unit cell structure are represented in Table 1. Figure 7 displays the results of the simulation of the reflection characteristics. The proposed design manifests the reflection characteristics for frequencies
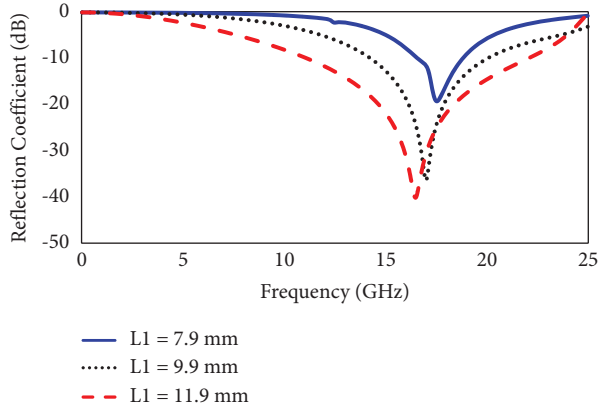
FIGURE 3: Simulated reflection coefficient of the proposed FSS for various values of $L1$.
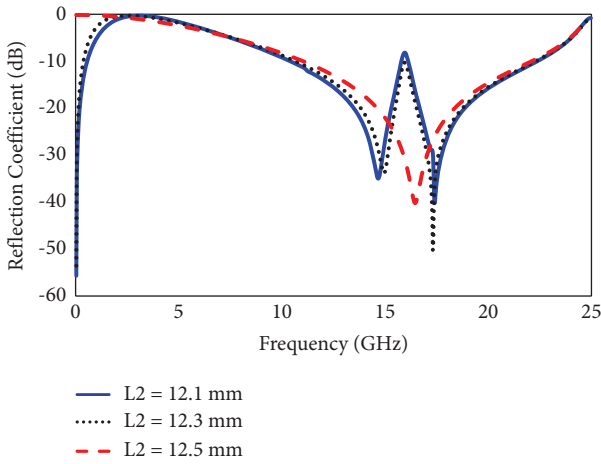

FIGURE 4: Simulated reflection coefficient of the proposed FSS for various values of $L2$.

FIGURE 5: Simulated reflection coefficient of the proposed FSS for various values of $R1$.

FIGURE 6: Simulated reflection coefficient of the proposed FSS for various values of $T1$.
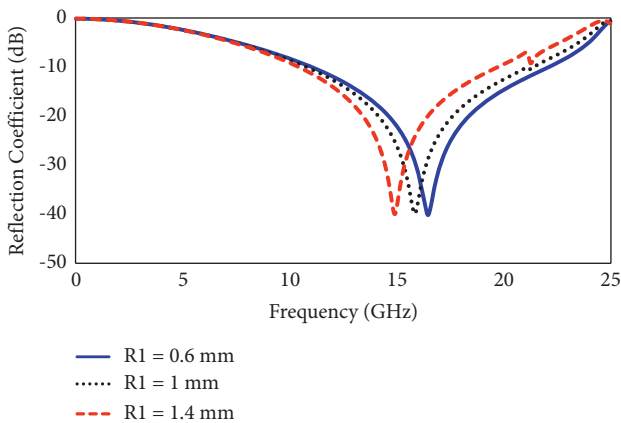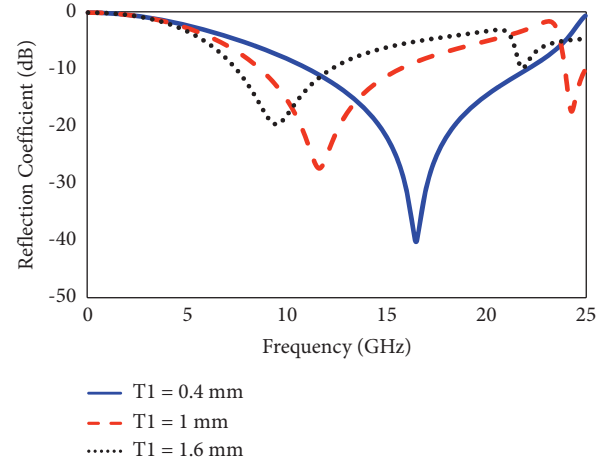
TABLE 1: Parametric analysis results for the dimension of $L1$, $L2$, $R1$, and $T1$.

S. no	Parameters	Unit cell (mm)	f lower (GHz)	f upper (GHz)	BW (GHz)	Fractional B.W (%)
1	$L1$ (mm)	7.9	16.6	18.8	2.2	12.429
		9.9	14.3	20.05	5.75	33.48
		11.9	11.075	22.075	11	66.36
2	$L2$ (mm)	12.1	10.45	22.35	11.9	72.5
		12.3	10.7	22.25	11.55	70.106
		12.5	11.075	22.075	11	66.36
3	$R1$ (mm)	0.6	11.075	22.075	11	66.36
		1.0	10.825	21.75	10.35	64.687
		1.4	10.475	19.675	9.2	61.028
4	$T1$ (mm)	0.4	11.314	21.898	10.584	63.74
		1.0	8.819	15.406	6.587	54.38
		1.6	7.585	11.973	4.388	44.87

3.1. Bandwidth Validation Using Fuzzy Logic Empirical Formula. The correctness of the fractional bandwidth is validated with the help of fuzzy logic. This method uses mathematical interpretations by varying the variables $R1$, $L1$, and $L2$ one at a time. The calculated fuzzy bandwidth is shown in Table 2. In Figure 8, empirical relations between fractional bandwidth and fuzzy bandwidth are presented.

3.2. Equivalent Circuit of the Proposed FSS. In the proposed FSS, the top-layer metallic square loop is modelled by a parallel RLC circuit with resistance $R1$, capacitance $C1$, and inductance $L1$. The unit cell's central square loop and circular conductor are separated by a gap, which is represented by $C3$. $L3$ represents the centre circular metallic ring. The FR4 substrate is modelled using the transmission line component based on the telegrapher model. The substrate has series inductance $L5$ and $L6$ and shunt capacitance $C5$ and $C6$. The proposed FSS equivalent circuit is presented in Figure 9(a). Similarly, $R2$, $C2$, and $L2$ represent the bottom-layer square loop. $C4$ represents

in a wide range from 11.075 GHz to 22.075 GHz by providing 11 GHz and a fractional bandwidth of 66.36%. The proposed FSS simulations $S11$ and $S21$ are presesnted in Figure 7.
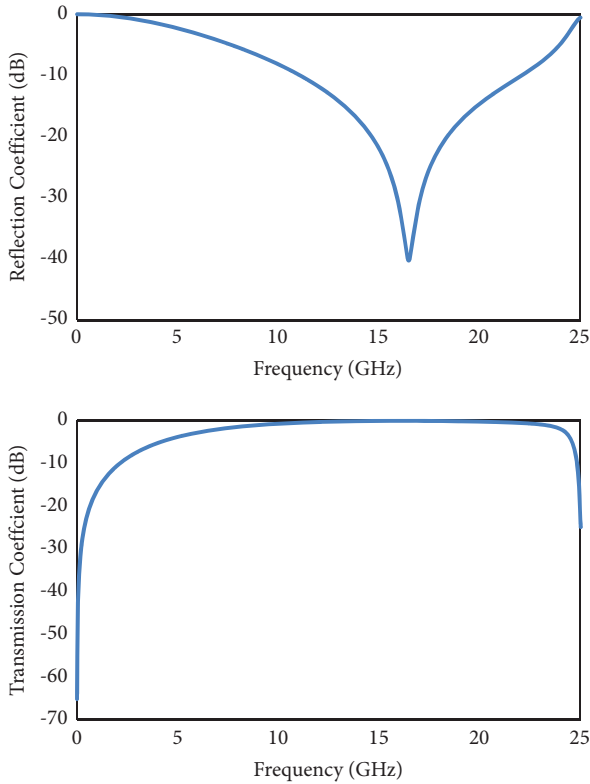
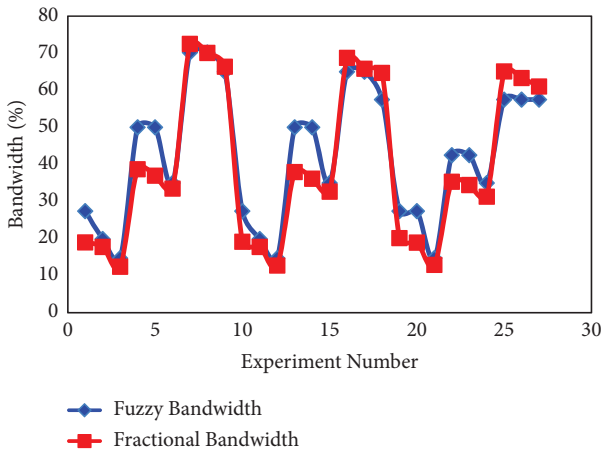FIGURE 7: Simulated results of S11 and S21 of the proposed design.

FIGURE 8: Empirical relations between fractional bandwidth and fuzzy bandwidth.

the gap, and *L4* represents the centre circular conductor. The equivalent circuit model's simulation results in the ADS tool are compared with the simulation results in CST and found small variation because of the lossy factor [31] is represented in Figure 9(b). The lumped element values are represented in Table 3.

Figure 10 depicts the proposed FSS's surface current and *E*-field distribution at the resonant frequency. The field distribution is taken under normal prevalence. The figure shows that more field is accumulated around the square loop and the centre circular conductor ring.

TABLE 2: Fractional and fuzzy bandwidth.

| S. no	L1 (mm)	L2 (mm)	R1 (mm)	Fractional BW (%)	Fuzzy BW (%)
1	3.95	6.05	0.6	18.988	27.4
2	3.95	6.15	0.6	17.77	19.9
3	3.95	6.25	0.6	12.429	14.7
4	4.95	6.05	0.6	38.73	50
5	4.95	6.15	0.6	36.98	50
6	4.95	6.25	0.6	33.48	35
7	5.95	6.05	0.6	72.5	70.2
8	5.95	6.15	0.6	70.106	70.2
9	5.95	6.25	0.6	66.36	65
10	3.95	6.05	1	19.14	27.4
11	3.95	6.15	1	17.77	19.9
12	3.95	6.25	1	12.747	14.7
13	4.95	6.05	1	37.98	50
14	4.95	6.15	1	36.17	50
15	4.95	6.25	1	32.66	35
16	5.95	6.05	1	68.759	65
17	5.95	6.15	1	65.834	65
18	5.95	6.25	1	64.687	57.5
19	3.95	6.05	1.4	20.134	27.4
20	3.95	6.15	1.4	18.92	27.4
21	3.95	6.25	1.4	12.9	14.7
22	4.95	6.05	1.4	35.34	42.5
23	4.95	6.15	1.4	34.46	42.5
24	4.95	6.25	1.4	31.318	35
25	5.95	6.05	1.4	65.112	57.5
26	5.95	6.15	1.4	63.341	57.5
27	5.95	6.25	1.4	61.028	57.5

This clearly shows that the area of the square loop and the circular ring is the reason for the passband characteristics.

4. Experimental and Measured Results

The simulated results of the proposed FSS are validated, and the prototype of the designed FSS is fabricated using the PCB photolithography thickness of various designs are compared using the wet etching method. The fabricated FSS is 300 mm × 300 mm and fabricated using FR4 substrate with 24 × 24-unit cells.

The total number of 564-unit cells fabricated on either side of the FR4 substrate and the proposed prototype is represented in Figure 11. In the mid of the RF absorbing wall, the fabricated FSS prototype is placed. It is excited by a transmitter horn antenna situated 2 metres apart and is received by a receiver horn antenna, respectively, as shown in Figures 12(a) and 12(b).

The absorbers in the RF absorbing wall avoid the measurement error by decreasing the EM diffraction at a large incident angle. In order to measure the range of frequency between 11.075 GHz and 22.075 GHz, two different kinds of horn antennas are used. The horn antenna used has an operating range between 1~12 GHz and 12~18 GHz. Figures 12(a) and 12(b) depict their corresponding measurement setup. The S11—reflection coefficient is measured as plotted in the figure, and the measured FBW is 64.15%. The fabrication error is the cause
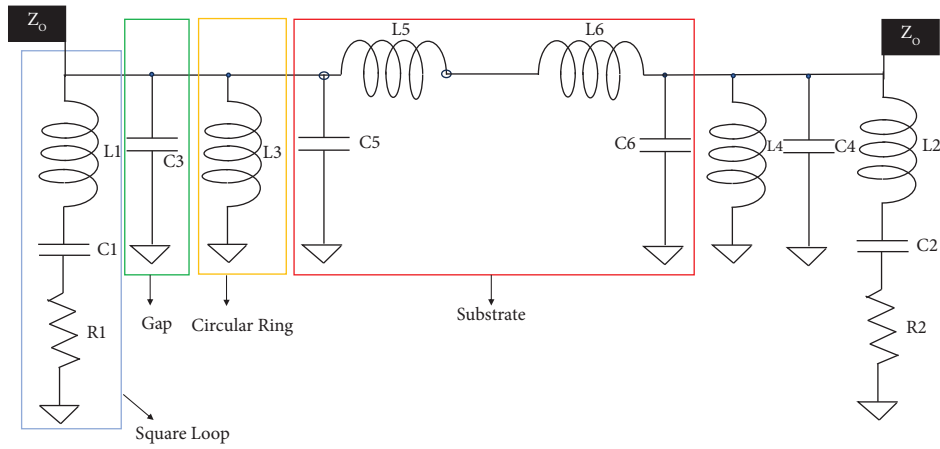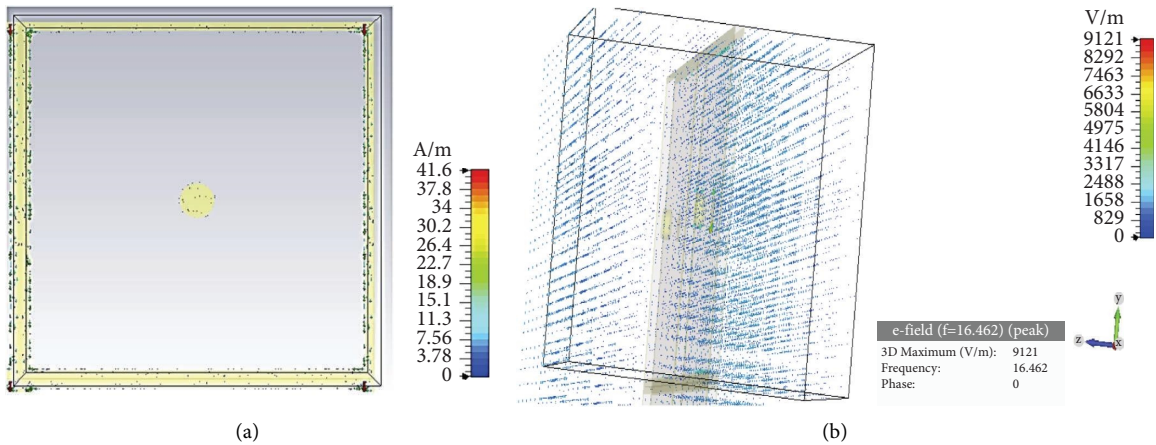
(a)
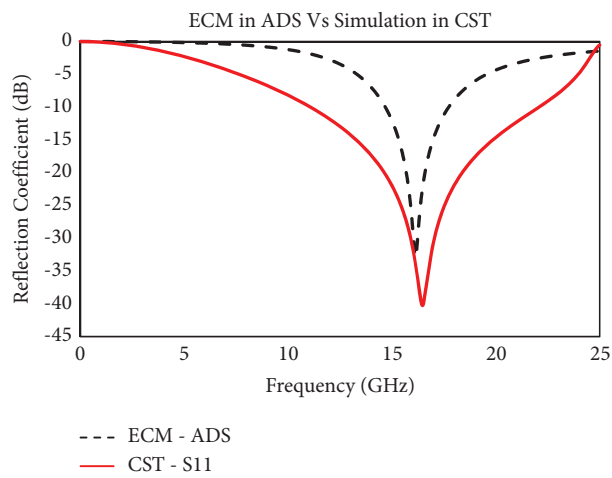
(b)

FIGURE 9: (a) Equivalent circuit of the proposed FSS. (b) Simulation results of $S11$—ECM in ADS vs. CST.

TABLE 3: Lumped elements value of ECM in ADS tool.

$L1, L2$ (nH)	$C1, C2$ (pF)	$R1, R2$ (Ω)	$C3, C4$ (pF)	$L3, L4$ (nH)	$C5, C6$ (pF)	$L5, L6$ (nH)
3.05	0.032	86	2.11	2.5	10.11	8.73

(a)

(b)

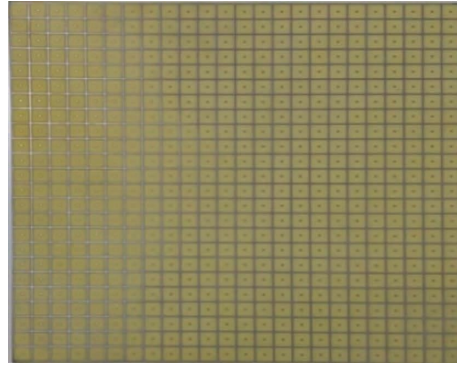FIGURE 10: (a) Surface current distribution. (b) E-field distribution.

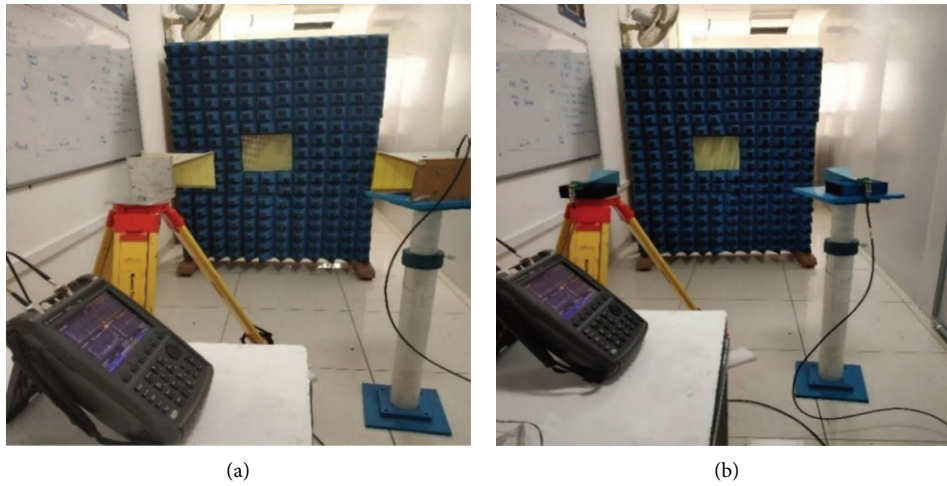FIGURE 11: Fabricated prototype of the proposed FSS.

(a)

(b)

FIGURE 12: (a) 1–12 GHz measurement setup (FSS) (b) 12–18 GHz measurement setup (FSS).
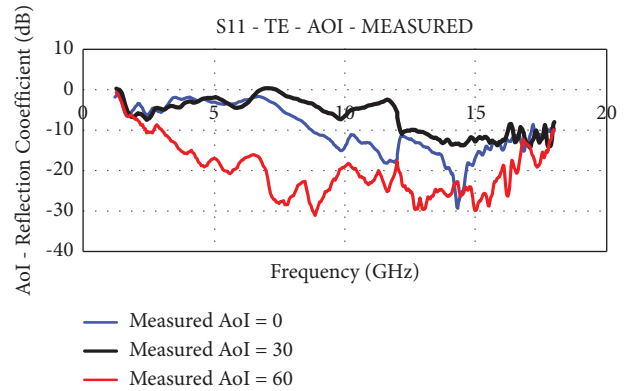

FIGURE 13: Comparison of simulated and measured results.

FIGURE 14: Measured AoI up to 60°.

of the small discrepancy between the measured and simulated findings. The comparison of the suggested FSS's simulated and measured reflection coefficients is shown in Figure 13. The measured AoI is represented in Figure 14, lower shift and a higher shift in the frequency are noted due to the fabrication impact.
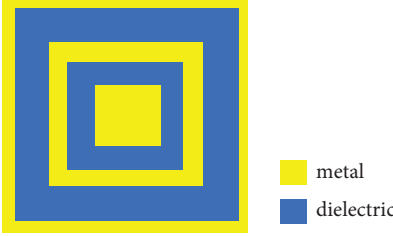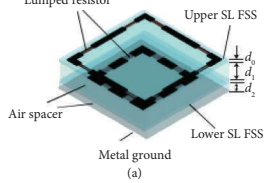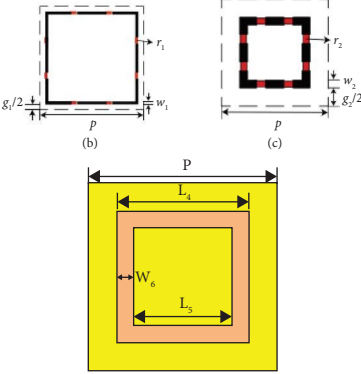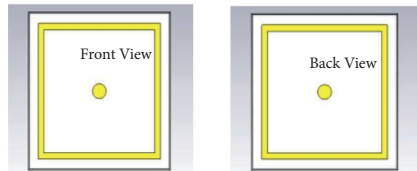
Table 4 demonstrates the comparison of the proposed work with existing work in the literature. The thickness of various designs is compared and reported as a 45% thickness reduction from the existing work. Table 5 is the proposed design structure which is associated with square loop and circular ring hence results in obtaining wideband frequency and is found to be novel compared to the literature.

The wavelength considered for computation in the comparison table concerns a lower cut-off frequency. Hence, it is

TABLE 4: Comparison of the proposed work with the existing work.

Ref	Number of conductive layers	Number of substrates	FBW %	Resonant frequency (GHz)	Unit cell size	Unit cell thickness (λ)
[17]	3	2	20.5	27.5	$(0.56\ \lambda_0)^2$	0.143
[18]	4	3	20	10	$(0.19\ \lambda_0)^2$	0.1
[25]	3	2	20	10	$(0.15\ \lambda_0)^2$	0.03
[32]	3	2	35	9.95	$(0.10\ \lambda_0)^2$	0.06
[33]	4	3	36.36	2.42	$(0.35\ \lambda_0)^2$	0.016
[34]	2	1	20	8.45	$(0.42\ \lambda_0)^2$	0.14
Proposed FSS	2	1	66.36	16.42	$(0.46\ \lambda_0)^2$	0.017

TABLE 5: Comparison of the structure with proposed and existing work.

Ref no.	Design structure	Structure type
[28]		Square loop and square slot
[35]		Resistor loaded square loop
[36]		Bottom side square loop
Proposed work		Square loop with ring in front and back side

more suitable for stealth applications as it demands reduction in thickness, compact design, minimum reflection, and reduced weight. The overall unit cell size is $0.46\ \lambda_0 \times 0.46\ \lambda_0$. The proposed work successfully achieves wide bandwidth and minimal thickness, which is the biggest hurdle for stealth applications. The designed FSS could be used for stealth, radomes, and EM shelter applications. As a future enhancement, conformal substrate can be used instead of FR4 substrate.

5. Conclusion

The unit cell size for the proposed single-layer FSS is $0.46\ \lambda_0 \times 0.46\ \lambda_0$. The proposed FSS structure well maintains stability in resonance due to its miniaturized unit cell. Apart from that, the metallic square loop and circular conductor exert considerable influence over the passband properties. Hence, the square loop's area is altered to achieve working frequency. On a FR4 substrate, the designed FSS is fabricated and preasured.

The proposed prototype is fabricated and measured; the measured results agree with the findings of simulations, validating the proposed structure. The proposed FSS resonates at 16.5 GHz, and it has good stability under various incident angles. The proposed work helps to reduce the reflections in the aircraft at a low cost, designed an FSS with minimum thickness for stealth applications and achieved wideband frequency. The proposed single-layer double Sided FSS is compact with a minimum thickness and covers X, Ku, and Ka bands with a fractional bandwidth of 66.36% as a wideband bandpass filter. The wide bandpass filter resonates in the X, Ku, and K band in the simulation since it is measured for 1–18 GHz, and the experimental result lies in the X and Ku band. The overall thickness is reduced. Furthermore, the FSS prototype shows a stable response for both polarizations. The designed and developed single-layer FSS includes the following features, which have been shown to be useful in applications for radars, EM shelters, and stealth.

Data Availability

No data were used to support this study.

Conflicts of Interest

The authors declare that they have no conflicts of interest.

References

[1] B. A. Munk, *Frequency Selective Surfaces: Theory and Design*, Wiley-Interscience, New York, NY, USA, 2000.

[2] Y. J. Lee, J. Yeo, R. Mittra, and W. S. Park, "Design of a High-Directivity Electromagnetic Band gap (EBG) resonator antenna using a frequency-selective surface (FSS) Superstrate," *Microwave and Optical Technology Letters*, vol. 43, no. 6, pp. 462–467, 2004.

[3] F. Costa and A. Monorchio, "A frequency selective radome with wideband absorbing properties," *IEEE Transactions on Antennas and Propagation*, vol. 60, no. 6, pp. 2740–2747, 2012.

[4] R. Gardelli, M. Albani, and F. Capolino, "Array thinning by using antennas in a Fabry-Perot cavity for gain enhancement," *IEEE Transactions on Antennas and Propagation*, vol. 54, no. 7, pp. 1979–1990, 2006.

[5] S. Chakravarty, R. Mittra, and N. R. Williams, "Application of a micro genetic algorithm (MGA) to the design of broadband microwave absorbers using multiple frequency selective surface screens buried in dielectrics," *IEEE Transactions on Antennas and Propagation*, vol. 50, no. 3, pp. 284–296, 2002.

[6] F. Costa, A. Kazemzadeh, S. Genovesi, and A. Monorchio, "Electro-magnetic absorbers based on frequency selective surfaces," *Forum for Electromagnetic Research Methods and Application Technologies (fermat)*, vol. 37, no. 1, pp. 1–23, 2016.

[7] Y. Li, L. Li, Y. Zhang, and C. Zhao, "Design and synthesis of multilayer frequency selective surface based on antenna-filter-antenna using Minkowski fractal structures," *IEEE Transactions on Antennas and Propagation*, vol. 63, no. 1, pp. 133–141, 2015.

[8] S. M. A. Momeni Hasan Abadi, M. Li, N. Behdad, and N. Behdad, "Harmonic-suppressed miniaturized-element frequency selective surfaces with higher order bandpass responses," *IEEE Transactions on Antennas and Propagation*, vol. 62, no. 5, pp. 2562–2571, 2014.

[9] Q. Lv, C. Jin, B. Zhang, and R. Mittra, "Wide-passband dual-polarized elliptic frequency selective surface," *IEEE Access*, vol. 7, pp. 55833–55840, 2019.

[10] A. Al-Sheikh and Z. Shen, "Design of wideband bandstop frequency selective structures using stacked parallel strip line arrays," *IEEE Transactions on Antennas and Propagation*, vol. 64, no. 8, pp. 3401–3409, 2016.

[11] S. S. Sampath and R. Sivasamy, "A single-layer UWB frequency-selective surface with band-stop response," *IEEE Transactions on Electromagnetic Compatibility*, vol. 62, no. 1, pp. 276–279, 2020.

[12] Q. Chen, D. Sang, M. Guo, and Y. Fu, "'Miniaturized frequency-selective rasorber with a wide transmission band using circular spiral resonator," *IEEE Transactions on Antennas and Propagation*, vol. 67, no. 2, pp. 1045–1052, 2019.

[13] Q. Lv, C. Jin, B. Zhang, and R. Mittra, "Wide-passband dual-polarized elliptic frequency selective surface," *IEEE Access*, vol. 7, pp. 55833–55840, 2019.

[14] Y. Shi, W. Zhuang, W. Tang, C. Wang, and S. Liu, "Modeling and analysis of miniaturized frequency selective surface based on 2.5-dimensional closed loop with additional transmission pole," *IEEE Transactions on Antennas and Propagation*, vol. 64, no. 1, pp. 346–351, 2016.

[15] T. Hussain, Q. Cao, J. K. Kayani, and I. Majid, "Miniaturization of frequency selective surfaces using 2.5-D knitted structures: design and synthesis," *IEEE Transactions on Antennas and Propagation*, vol. 65, no. 5, pp. 2405–2412, 2017.

[16] J. Zhu, W. Tang, C. Wang, C. Huang, and Y. Shi, "Dual-polarized bandpass frequency-selective surface with quasi-elliptic response based on square coaxial waveguide," *IEEE Transactions on Antennas and Propagation*, vol. 66, no. 3, pp. 1331–1339, 2018.

[17] D. Li, T.-W. Li, R. Hao et al., "A low-profile broadband bandpass frequency selective surface with two rapid band edges for 5G near-field applications," *IEEE Transactions on Electromagnetic Compatibility*, vol. 59, no. 2, pp. 670–676, 2017.

[18] X. Liu, Q. Wang, W. Zhang, M. Jin, and M. Bai, "On the improvement of angular stability of the 2nd-order miniaturized FSS structure," *IEEE Antennas and Wireless Propagation Letters*, vol. 15, pp. 826–829, 2016.

[19] W. Li and Y. Li, "A high selectivity, miniaturized low profile dual-band bandpass FSS with a controllable transmission zero," *International Journal of Antennas and Propagation*, vol. 2017, Article ID 7983567, 9 pages, 2017.

[20] L.-L. Yang, X.-C. Wei, D. Yi, and J.-M. Jin, "A bandpass frequency selective surface with a low cross-polarization based on cavities with a hybrid boundary," *IEEE Transactions on Antennas and Propagation*, vol. 65, no. 2, pp. 654–661, 2017.

[21] N. Behdad, M. Al-Joumayly, and M. Salehi, "A low-profile third order bandpass frequency selective surface," *IEEE Transactions on Antennas and Propagation*, vol. 57, no. 2, pp. 460–466, 2009.

[22] Y. Ma, W. Wu, Y. Yuan, W. Yuan, and N. Yuan, "A high-selective frequency selective surface with hybrid unit cells," *IEEE Access*, vol. 6, pp. 75259–75267, 2018.

[23] Y. Ma, W. Wu, Y. Yuan, X. Zhang, and N. Yuan, "A wideband FSS based on vias for communication systems," *IEEE Antennas and Wireless Propagation Letters*, vol. 17, no. 12, pp. 2517–2520, 2018.

[24] X. Liu, Q. Wang, W. Zhang, M. Jin, and M. Bai, "On the improvement of angular stability of the 2nd-order

miniaturized FSS structure," *IEEE Antennas and Wireless Propagation Letters*, vol. 15, pp. 826–829, 2016.

[25] M. Al-Joumayly and N. Behdad, "A new technique for design of low-profile second-order bandpass frequency selective surfaces," *IEEE Transactions on Antennas and Propagation*, vol. 57, no. 2, pp. 452–459, 2009.

[26] P.-C. Zhao, Z.-Y. Zong, W. Wu, and D. G. Fang, "A convoluted structure for miniaturized frequency selective surface and its equivalent circuit for optimization design," *IEEE Transactions on Antennas and Propagation*, vol. 64, no. 7, pp. 2963–2970, 2016.

[27] S. Narayan, G. Gulati, B. Sangeetha, and R. U. Nair, "Novel metamaterial-element based FSS for airborne radome applications," *IEEE Transactions on Antennas and Propagation*, vol. 66, no. 9, pp. 4695–4707, 2018.

[28] J. Pae, S. Im, Y. Han, and K. Song, "Analysis and design of a single layer double square slot frequency selective surface with single stopband between double passbands," *Engineering Reports*, vol. 4, no. 12, 2022.

[29] R. S. Anwar, L. Mao, and H. Ning, "Frequency selective surfaces: a review," *Applied Sciences*, vol. 8, no. 9, p. 1689, 2018.

[30] D. Kanchana, S. Radha, B. S. Sreeja, and E. Manikandan, "A single layer UWB frequency selective surface for shielding application," *Journal of Electronic Materials*, vol. 49, no. 8, pp. 4794–4800, 2020.

[31] D. Kanchana, S. Radha, and B. S. Sreeja, "A miniaturised FSS with band-stop response for shielding application in X-band frequency," *Pramana*, vol. 96, no. 1, p. 29, 2022b.

[32] M. Yan, S. Qu, J. Wang et al., "A miniaturized dual-band FSS with second order response and large band separation," *IEEE Antennas and Wireless Propagation Letters*, vol. 14, pp. 1602–1605, 2015.

[33] P.-C. Zhao, Z.-Y. Zong, W. Wu, B. Li, and D. G. Fang, "'Miniaturized-element bandpass FSS by loading capacitive structures," *IEEE Transactions on Antennas and Propagation*, vol. 67, no. 5, pp. 3539–3544, 2019.

[34] C. Jin, Q. Lv, J. Wang, and Y. Li, "'Capped dielectric inserted perforated metallic plate bandpass frequency selective surface," *IEEE Transactions on Antennas and Propagation*, vol. 65, no. 12, pp. 7129–7136, 2017.

[35] Y. Zhi-Xin, X. Shao-Qiu, Y. Li, and B. Wang, "On the design of wideband absorber based on multilayer and multiresonant FSS array," *IEEE Antennas and Wireless Propagation Letters*, vol. 20, no. 3, pp. 284–288, 2021.

[36] A. Parameswaran, D. Kundu, and H. S. Sonalikar, "A dual-polarized wideband frequency-selective rasorber with low in-band insertion loss and high oblique incidence stability," *IEEE Transactions on Electromagnetic Compatibility*, vol. 63, no. 6, pp. 1820–1828, 2021.